



COASTAL FLOOD INUNDATION MONITORING WITH SATELLITE C-BAND AND L-BAND SYNTHETIC APERTURE RADAR DATA¹

Elijah Ramsey III, Amina Rangoonwala, and Terri Bannister²

ABSTRACT: Satellite Synthetic Aperture Radar (SAR) was evaluated as a method to operationally monitor the occurrence and distribution of storm- and tidal-related flooding of spatially extensive coastal marshes within the north-central Gulf of Mexico. Maps representing the occurrence of marsh surface inundation were created from available Advanced Land Observation Satellite (ALOS) Phased Array type L-Band SAR (PALSAR) (L-band) (21 scenes with HH polarizations in Wide Beam [100 m]) data and Environmental Satellite (ENVISAT) Advanced SAR (ASAR) (C-band) data (24 scenes with VV and HH polarizations in Wide Swath [150 m]) during 2006-2009 covering 500 km of the Louisiana coastal zone. Mapping was primarily based on a decrease in backscatter between reference and target scenes, and as an extension of previous studies, the flood inundation mapping performance was assessed by the degree of correspondence between inundation mapping and inland water levels. Both PALSAR- and ASAR-based mapping at times were based on suboptimal reference scenes; however, ASAR performance seemed more sensitive to reference-scene quality and other types of scene variability. Related to water depth, PALSAR and ASAR mapping accuracies tended to be lower when water depths were shallow and increased as water levels decreased below or increased above the ground surface, but this pattern was more pronounced with ASAR. Overall, PALSAR-based inundation accuracies averaged 84% ($n = 160$), while ASAR-based mapping accuracies averaged 62% ($n = 245$).

(KEY TERMS: remote sensing; ENVISAT ASAR; ALOS PALSAR; coastal marshes; storm surge; tidal inundation.)

Ramsey III, Elijah, Amina Rangoonwala, and Terri Bannister, 2013. Coastal Flood Inundation Monitoring with Satellite C-band and L-band Synthetic Aperture Radar Data. *Journal of the American Water Resources Association* (JAWRA) 1-22. DOI: 10.1111/jawr.12082

INTRODUCTION

Even though flood-extent mapping has become a routine activity in coastal marsh and forested wetland landscapes (Lu and Kwoun, 2008; Ramsey *et al.*, 2011, 2012), particularly during and after extreme storm events, satellite-based observations of long-term

effects of flooding on natural vegetation are less common, especially those effects requiring high temporal frequency observations over large coastal extent. As reported in Ramsey *et al.* (2009b, 2012), the combined use of Environmental Satellite (ENVISAT) Advanced SAR (ASAR) and Landsat Thematic Mapper (TM) optical imagery provided synergistic observations to document the extent of the coastal surge

¹Paper No. JAWRA-12-0171-P of the *Journal of the American Water Resources Association* (JAWRA). Received July 27, 2012; accepted February 27, 2013. © 2013 American Water Resources Association. This article is a U.S. Government work and is in the public domain in the USA. **Discussions are open until six months from print publication.**

²Respectively, Principal Investigator (Ramsey III), U.S. Geological Survey, National Wetlands Research Center, 700 Cajundome Blvd., Lafayette, Louisiana 70506; Remote Sensing Researcher (Rangoonwala) and Spatial Analysis Researcher (Bannister), Five Rivers Services, LLC, Colorado Springs, Colorado 80918 (E-Mail/Ramsey III: ramseye@usgs.gov).

Re-use of this article is permitted in accordance with the Terms and Conditions set out at http://wileyonlinelibrary.com/onlineopen#OnlineOpen_Terms

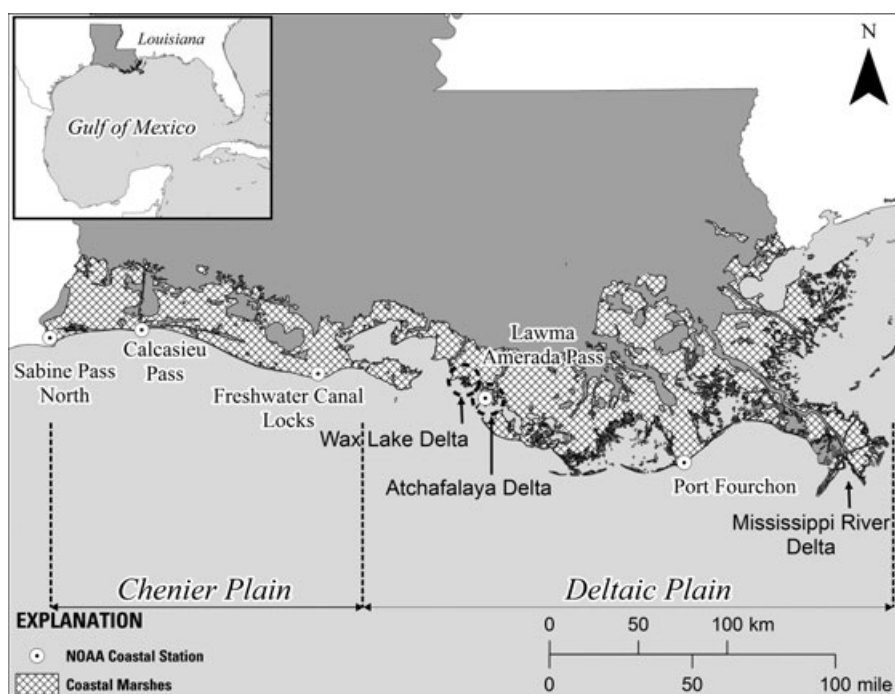


FIGURE 1. Study Area Covering the Coastal Marshes of Louisiana, as well as Locations of NOAA Coastal Stations (water-level gages) (NOAA, 2010).

accompanying Hurricane Ike and the resultant marsh dieback. Because of the comparable inundation information, the dieback could be directly attributed to prolonged waterlogging and elevated salinity levels. This connection illustrated how inundation monitoring with frequent satellite-based radar data observations, combined with cloud-free optical data, can provide direct linkages between vegetation condition and the primary physical forces controlling it. The next step extended our study to include the distribution and occurrence of both storm- and tidal-related flooding of spatially extensive coastal marshes.

Satellite Synthetic Aperture Radar (SAR) was evaluated as a method to provide the operational flood inundation monitoring of a 500-km long coastal region within the north-central Gulf of Mexico (GOM) (Figure 1). The evaluation emphasized high temporal frequency preparation of inundation distribution maps covering coastal Louisiana. The research included data collected operationally by the Phased Array type L-Band SAR (PALSAR) sensor onboard the Japan Aerospace Exploration Agency (JAXA) Advanced Land Observation Satellite (ALOS), which operated from January 2006 to April 2011 and the ASAR sensor onboard the European Space Agency (ESA) ENVISAT which operated from March 2002 to April 2012. The wide use of these satellite SAR sensors during their lifetimes provided the maximum temporal frequency of data collections of the Louisiana coastal zone. An added advantage was the ability

to compare the performance of two widely used SAR sensor systems operating at different frequencies or wavelengths; the L-band PALSAR at HH (horizontal send and receive) polarization and the C-band ASAR at HH and VV (vertical send and receive) polarizations. SAR systems operating at both L-band and C-band have proven capable of mapping inundation in coastal and river floodplain systems (Ormsby *et al.*, 1985; Ramsey *et al.*, 1994; Leconte and Pultz, 1991; Hess *et al.*, 1995; Ramsey, 1995; Dobson *et al.*, 1996; Pope *et al.*, 1997; Smith, 1997; Werle *et al.*, 2000; Kasischke *et al.*, 2003; Wang, 2004; Kiage *et al.*, 2005; Töyra and Pietroniro, 2005; Henry *et al.*, 2006; Matgen *et al.*, 2007; Lang *et al.*, 2008; Hong *et al.*, 2010).

The Importance of Satellite-Based Strategic Inundation Mapping in Coastal Regions

The coastal zone of Louisiana, located in the central-northern GOM, accounts for about 40% of coastal wetlands in the continental United States (Neyland, 2007). As in most coastal zones that include expanses of marsh, the zone is characterized by a gradual increase of elevation that starts at sea level and reaches 1-1.5 m at the southern extent of upland prairie and forests. In addition to flood events (Kiage *et al.*, 2005; Ramsey *et al.*, 2009b), tidal flushing, seasonal and interannual marsh phenology (Wang, 2004), and the ephemeral nature of many small water

bodies (Kiage *et al.*, 2005) produce a highly dynamic landscape. Rapid changes within the landscape must be accounted for to precisely identify the threshold duration of saturation required for wetland viability (Lang *et al.*, 2008). While limited results do not allow immediate inference on health or trend of the marsh system, evidence suggests that episodic events can cause severe stress on marsh vegetation in the region (Ramsey *et al.*, 2009b, 2012). Produced systematically, maps portraying wetland vegetation condition and spatially distributed inundation could provide crucial information for linking wetland health with flood frequency and duration (Hess *et al.*, 1995; Ramsey, 1995; Kasischke *et al.*, 2003; Töyra and Pietroniro, 2005).

Point Measurements, Hydraulic Models, and Inundation Mapping

Conventional contour mapping of water-level point measurements is hampered by the high spatial variability of flood occurrences, difficulties in timing field data collections with highly dynamic flood events, and inherent problems in predicting marsh flood stage from off-site gages (Leconte and Pultz, 1991; Ramsey, 1995). Although automated contouring advancements have successfully delineated flood inundation in SAR scenes (e.g., Horritt *et al.*, 2001), in coastal mapping, the necessary contrast between flooded and non-flooded pixels in the SAR scene for successful automated contouring is largely lacking (Ramsey *et al.*, 2011, 2012). Hydraulic flow models can alleviate many difficulties inherent in contouring (Smith, 1997); however, as in contouring, the lack of the necessary spatial density of flood-stage measurements and the prevalent disconnect between marsh and off-site measured flows diminish the capability to provide calibration and validation of predicted flood inundation patterns (Kasischke *et al.*, 2003; Matgen *et al.*, 2007). Remote sensing systems are used to help overcome these difficulties in monitoring and simulating the spatially distributed and rapidly changing nature of coastal flood inundation.

Optical and SAR-Based Inundation Mapping

Remote sensing with passive optical sensors can adequately address many coastal resource management issues (Klemas *et al.*, 1993; Smith, 1997; Lunetta *et al.*, 1998), particularly when associated with changes in leaf pigment concentrations reflected as spectral variability (Ramsey and Rangoonwala, 2006; Ramsey *et al.*, 2009a). However, the dependence of optical remote sensing systems on sunlight and favorable weather conditions critically limits their

usefulness when time-constrained collections are needed (Hess *et al.*, 1995; Smith, 1997; Kasischke *et al.*, 2003; Ramsey, 2005; Töyra and Pietroniro, 2005; Lang *et al.*, 2008). Even when reliance on time-constrained collections is minimized, the restricted penetration of visible and near-infrared radiation into full cover canopies limits detection of subcanopy flooding with optical systems (Ormsby *et al.*, 1985; Moghaddam *et al.*, 2003; Töyra and Pietroniro, 2005).

Microwave-based remote sensing systems offer a viable alternative data source when timely and consistent collections are dominant concerns (Kasischke *et al.*, 2003; Ramsey *et al.*, 2006; Matgen *et al.*, 2007; Lu and Kwoun, 2008). SAR sensors operating at centimeter wavelengths can collect information day and night and in most weather conditions and can provide increased canopy penetration (Ormsby *et al.*, 1985; Hess *et al.*, 1995; Lewis *et al.*, 1998; Ramsey, 2005; Töyra and Pietroniro, 2005). Satellite-based radar sensors, such as the C-band ASAR aboard ENVISAT, the C-band SAR aboard the Canadian's Radarsat, the X-band SAR aboard the German TerraSAR-X, and the L-band PALSAR aboard the Japanese ALOS, have proven to be valuable tools for surveying land and water surfaces during weather-related emergencies (Symbios Spazio, 2010).

SAR-Based Detection of Marsh Subcanopy Flooding

Although increased canopy transmittance of longer wavelengths implies superior subcanopy inundation mapping with SAR systems operating at L-band frequency (Ramsey, 1998; Kasischke *et al.*, 2003; Töyra and Pietroniro, 2005), the C-band sensor has performed well in mapping Louisiana marshes, as it has in other marshes occupying the northern and eastern GOM coasts (Ramsey, 1995; Kasischke *et al.*, 2003; Kiage *et al.*, 2005; Ramsey *et al.*, 2009b) and elsewhere (Hess *et al.*, 1995; Werle *et al.*, 2000). C- and L-band SAR data in HH and VV polarizations (acquired by the Shuttle Imaging Radar-C platform) were used by Pope *et al.* (1997) to demonstrate that flooding of herbaceous vegetation can be exhibited as an increase or decrease in SAR backscatter. In effect, the nature of the change and the ability to differentiate between flooded and non-flooded marshes depends on the marsh type, height, density, stem orientation and size, soil moisture, inundation depth and history, as well as the SAR sensor parameters (Pope *et al.*, 1997; Kasischke *et al.*, 2003; Grings *et al.*, 2005).

In coastal marshes, the interrelation between the biophysical variables and incident SAR C-band signals identified by Pope *et al.* (1997) dominantly produce a backscatter decrease from flooded *vs.* non-flooded marshes (Ramsey, 1995; Dobson *et al.*,

1996; Kasischke *et al.*, 2003). In the north-central GOM, Kiage *et al.* (2005) used C-band SAR with HH polarization (acquired by Radarsat) to document decreased backscatter from hurricane surge-flooded saline, brackish, and fresh coastal marshes, compared to presurge backscatter intensities. In addition, any polarization influence on the effectiveness of flood mapping (e.g., Grings *et al.*, 2005) was expected to favor the copolarization (VV and HH) SAR data applied in this study as compared to cross-polarization (HV and VH) SAR data (e.g., Smith, 1997). Trends observed and modeled in fresh to saline coastal marshes in the northern GOM have consistently documented decreased HH and VV SAR backscatter from flooded *vs.* non-flooded marshes.

Collection Strategies and Inundation Mapping

Sampling Frequency. Detecting and quantifying long-term environmental trends for resource monitoring and short-term dramatic change for emergency response rely on consistent and sequential (systematic) data collection. The frequency of the data collection determines if the dynamics of the feature of interest are either captured or missed (Klemas, 2005). For instance, coastal resource phenologies should be imaged weekly and coastal flooding every 2 h or better. A 2-h revisit frequency is not feasible with operational satellite systems; however, if systematic sampling is available, higher frequency sampling may be approximated (Hager *et al.*, 2009). For example, if the collections occur weekly or bi-monthly over a long period, the tidal stages and inland extents at the times of each collection may be combined with topographic information to construct hypsometric curves that approximate the relationship between stage and flood extent over a tidal period (e.g., Ramsey *et al.*, 1998). As independent measures, these inundation patterns can provide direct calibration and validation of hydraulic flow models that account for astronomical forcing as well as variable surface stress, bottom friction, non-tidal inputs, and others.

Synoptic Coverage *vs.* Spatial Resolution. There is a trade-off between spatial resolution and repeat frequency such that the higher the temporal frequency of scene collection, the coarser is the ground spatial resolution (e.g., Schaber and Badeck, 2003; Fisher and Mustard, 2007). For example, large-format SAR collections at bimonthly to weekly or better repeat frequencies primarily provide moderate spatial resolutions (e.g., 150 m or less) (Hager *et al.*, 2009). While large-format monitoring provides a regional synoptic view, rapid response, and early detection of change, modes having a moderate swath

(e.g., 60 km) and higher ground spatial resolution (e.g., 25-m pixel) may enhance flood detection by decreasing the variety of features within the pixel, thereby lowering classification confusion. These features include scattered ponding of flood waters (Ramsey *et al.*, 1998) and variable stand-level canopy structures (e.g., canopy gaps, subcanopy species mixtures) (Ramsey *et al.*, 2004). Conversely, there is the possibility that high-frequency collections at finer spatial scales detailing the high spatial variability can obscure the detection of change (e.g., Schaber and Badeck, 2003; Fisher and Mustard, 2007). The exact interrelationship between the spatial extent, ground resolution, and temporal factors and the flood detection performance was not determined in this study; however, the dynamics of coastal flooding and the operational prerequisite of monitoring an extensive coastal region required a high temporal data source with reasonable spatial extent and ground resolution.

Objectives

The goal of this applied research was to demonstrate the ability of SAR satellite imagery to operationally monitor the distribution and occurrence of storm- and tidal-related flooding covering the spatially extensive Louisiana coastal marshes. A necessary requirement of the flood-detection strategy was that it be based upon routine measurements that are cost effective and easily implemented into operational resource management and that it was verified and calibrated with operational ground-based measurements (Nielsen and Werle, 1993). To fulfill that goal while adhering to the set product requirement, we based the coast-wide flood detection demonstration on 45 available large-format (100- and 150-m ground resolution) SAR scenes from late 2006 to September 2009 that individually covered at least half the Louisiana coastal zone (Figure 1). The objectives were to:

1. derive inundation distributions from available SAR scenes,
2. document limitations and successes of large-format SAR-based inundation mapping, and
3. assess the Coastwide Reference Monitoring System (CRMS) hydrologic water-level database (SONRIS, 2009) with respect to the validation of the SAR-based inundation mapping.

Study Area

The study area included estuarine and palustrine wetlands stretching from the western chenier to the eastern deltaic plains of coastal Louisiana (Sasser

et al., 2008), located in the north-central GOM (Figure 1). The deltaic plain was formed and is primarily sustained by the direct deposition of Mississippi River sediments, while the chenier plain is primarily dependent on current-related reworking of sediments from the Atchafalaya River (<http://www.mvd.usace.army.mil/lcast/pdfs/CEM2.pdf>). Relationships between water and sediment gave rise to highly permeable sand and shell (chenier) barriers in the west and barrier islands in the east that protect extensive back-barrier marshes that extend inland from 6 to 24 km, commonly at less than 1.5 m above mean sea level and with slopes of less than 0.2 m/km (Chabreck, 1970).

The Louisiana coastal marsh zone is dominantly underlain by frequently saturated soils. In this zone, subsurface faulting can produce surface subsidence that results in marsh submergence and fragmentation and ultimately, the formation of permanent water bodies (Kiage *et al.*, 2005; Morton *et al.*, 2005). In addition, hurricanes scour the marsh, creating small water bodies (Neyland, 2007), and push water with elevated salinity into freshwater marshes, causing salt burn in those areas (Neyland, 2007; Ramsey *et al.*, 2009b). Aggravating these detrimental impacts are channels and levees, as well as impoundments constructed to provide transport conduits and waterfowl sanctuaries that impede overland flow. These impediments can lengthen the marsh exposure to elevated salinity water and in the case of intense rainfall accompanying storm events, prolong inundation that promotes waterlogging and subsequent marsh alteration and deterioration. The combination of low topographic relief, poorly drained soils, tectonic activity, and flow impedance creates a spatially complex hydrological landscape.

METHODS

Collecting, Calibrating, and Georeferencing Satellite Data

The SAR coverage was obtained with the L-band PALSAR sensor aboard the Japanese ALOS and the C-band ASAR sensor onboard ENVISAT satellites. PALSAR and ASAR scenes were selected from the archival record with three objectives in mind. First, because it required two adjacent scenes to cover the entire Louisiana coastline, dominantly, scenes that were part of an adjacent scene pair collected close in time were selected. Second, to provide a good temporal sampling, scene pair selection was prioritized to monthly or at least seasonal frequency. Third, because reference scenes were required to create the inundation maps, special attention was taken to

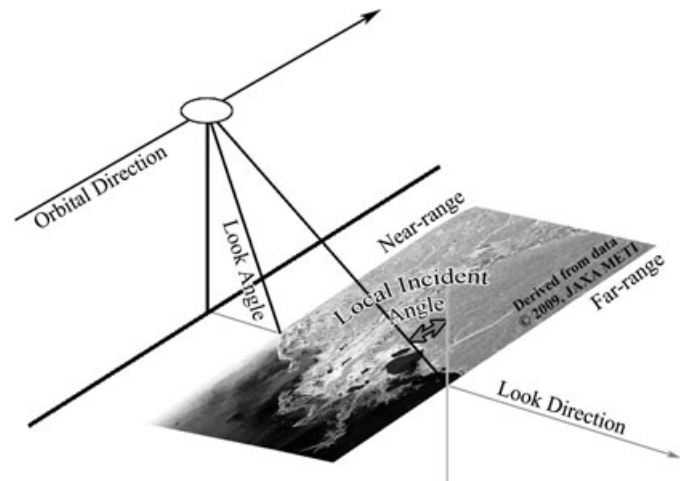


FIGURE 2. SAR Swath Coverage Depicting Collection and Scene Geometries. The example scene in the diagram was captured by the PALSAR sensor aboard ALOS (©2009, JAXA METI).

identify reference scenes that enhance the performance of the inundation mapping.

The PALSAR scenes were collected in Wide Area Observation mode (Burst Mode 1 [WB1]) at a nominal spatial resolution of 100 m and incidence angles of 18° in the near-range to 43° in far-range of the imaged swath (e.g., Figure 2). All PALSAR scenes used in this study were collected in the descending orbit (Figure 3a; Table 1). To allow scene-to-scene comparability, the HH polarized PALSAR scenes were radiometrically calibrated to sigma naught backscattering coefficient (σ_0) with MapReady Remote Sensing Software available at the Alaska Satellite Facility website (www.asf.alaska.edu/sardatacenter/softwaretools). The 21 PALSAR scenes selected from January 2007 through September 2009 included all WB1 PALSAR scenes collected over coastal Louisiana during that time period (Figure 3a; Table 1).

The ASAR scenes were collected in Wide Swath mode at a nominal spatial resolution of 150 m and incidence angles of 17° in the near-range to 42° in far-range of the imaged swath. The ASAR scenes were collected in both the ascending and descending orbits (Figures 3b and 3c; Table 1). The HH- and VV-polarized ASAR scenes were transformed to σ_0 estimates by using Next ESA SAR Toolbox (NEST) software and calibration coefficients provided by the ESA (2007). The 24 ASAR scenes selected were collected from July 2006 to September 2009 and represented a wide range of sea levels and tidal flushing.

All SAR satellite data were registered to a Landsat TM Lambert Conformal Conic (LCC) 25-m spatial resolution base image. The LCC projection eliminated problems of multiple Universal Transverse Mercator zones and matched the Louisiana State Plane Coordinate System. The LCC projection (WGA84 geoid) used

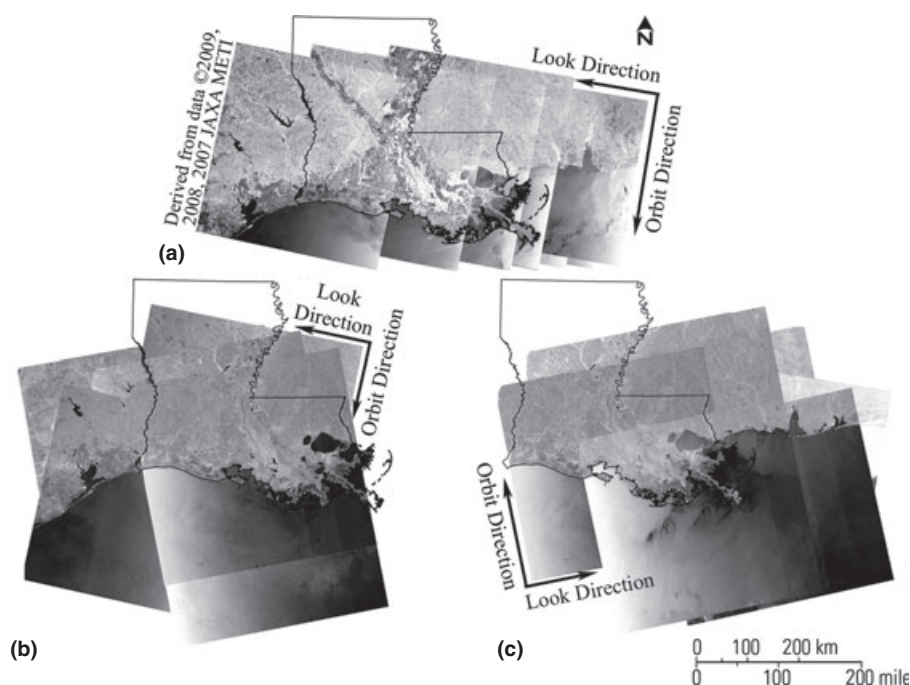


FIGURE 3. (a) ALOS PALSAR, and ENVISAT ASAR (b) HH and (c) VV Coverages. The descending orbit direction was from north to south looking toward the west. The ascending orbit direction was from south to north looking toward the east.

two standard parallels separated by 1.5° latitude, a central meridian, and a false northing and easting defined by the Southern Louisiana State Plane Coordinate System. Applying State Plane parameters, we found that areas projected with LCC *vs.* Albers Equal Area Conic differed by $<0.01\%$. In addition, the base TM projection was assessed by comparison to direct U.S. Geological Survey (USGS) Digital Orthophoto Quarter Quadrangles (DOQQs). Rectification errors of the LCC base TM to the DOQQs were most often less than 0.5 pixels and registration errors of the SAR scenes to the LCC base TM image were between 0.2 and 0.5 pixels. All SAR scenes were resampled to a 75-m pixel size as part of the registration.

Collecting Coastal and Inland Hydrologic Data

Coastal water-level timing and height records were obtained from the NOAA National Ocean Service Center for Operational Oceanographic Products and Services Operational Data Interactive Navigation (NOAA, 2010) for five hydrologic stations. These are located along the eastern (Port Fourchon), central (Freshwater Canal Locks and Lawma-Amerada Pass), and western (Sabine Pass North, and Calcasieu Pass) Louisiana coast (Figure 1).

Inland water-level data for calibrating and validating the inundation maps were obtained from the Strategic Online Natural Resources Information System (SONRIS) from the Louisiana Department of Natural Resources (SONRIS, 2009). A list of 212 hydro-

logic stations for which hydrographic records were available and suitable for our inundation analysis was obtained from the CRMS program (SONRIS, 2009).

Before initiating the final phase of inundation mapping, we assessed these 212 hydrographic records based on the following criteria. First, the water-levels needed to be referenced to the marsh surface (ground surface of marsh referenced at 0 m). Second, the records needed to reflect continuity and reliability. Continuity was exhibited by there being continuous records over the study period. Reliability was expressed by the nature of the hydrograph through time. For instance, if the water levels became near constant for a continued time period, recordings at that site became suspect and were compared to other inland sites. If the suspect records were abnormal when compared to those for other sites, the station was excluded from the validation analysis. Next, the remaining stations were assessed for the appropriateness of their locations for SAR inundation mapping.

Assessing Hydrologic Station Locations. The location of many hydrologic stations did not allow direct comparison between recorded water levels and surface inundation as calculated with SAR data. Most sites were located in water channels that can exhibit different flow dynamics than those of the marsh platform and were separated from the marsh platform by varying distances and obstructions, such as levees (e.g., Figures 4a and 4b) decoupling measured water levels from flooding occurring within the marsh platform.

TABLE 1. (a) Collected ALOS PALSAR WB1 and (b) ENVISAT ASAR WS Scenes.

(a) ALOS PALSAR WB1 Scenes							
Date	Path	Coverage	Pol.	Date	Path	Coverage	Pol.
2007				2008			
January-7	D. 487	East	HH	January-10	D. 487	East	HH
January-12	D. 490	West	HH	January-15	D. 490	West	HH
February-22	D. 487	East	HH	July-24	D. 485	East	HH
July-10	D. 487	East	HH	September-8	D. 485	East	HH
July-15	D. 490	West	HH	September-25	D. 486	East	HH
August-25	D. 487	East	HH	October-7	D. 484	East	HH
August-30	D. 490	West	HH	2009			
October-10	D. 487	East	HH	January-12	D. 487	East	HH
October-15	D. 490	West	HH	January-17	D. 490	West	HH
October-25	D. 487	East	HH	January-22	D. 493	West	HH
November-30	D. 490	West	HH	September-16	D. 488	East	HH
(b) ENVISAT ASAR WS Scenes							
Date	Path	Coverage	Pol.	Date	Path	Coverage	Pol.
2006				2009			
July-27	A. 434	West	HH	March-11	A. 119	East	VV
2007				March-30	A. 391	West & East	HH
July-25	A. 119	East	HH	April-2	A. 434	West	HH
July-31	A. 205	West	HH	May-17	D. 83	West	VV
September-4	A. 205	West	VV	May-20	A. 119	East	VV
September-14	A. 348	East	VV	May-20	D. 126	West	VV
2008				May-23	A. 162	West & East	VV
July-28	A. 391	East	VV	May-27	D. 226	East	VV
August-3	A. 477	West	VV	June-24	A. 119	East	HH
August-29	A. 348	East	VV	June-27	A. 162	West & East	HH
September-1	A. 391	East	VV	August-30	D. 83	East	VV
September-1	D. 398	West	VV	September-2	D. 269	East	VV
September-14	D. 83	West	VV				
September-17	A. 119	East	VV				

Notes: A, Ascending mode; D, descending mode; Pol., polarization.

Many sites were located in a mixed marsh and forest-stand landscape or were located in deteriorating marsh containing a high proportion of open water (e.g., Figures 4c and 4d) degrading the inundation performance based on decreased backscatter from flooded marshes. The contamination of the SAR pixel by mixed non-marsh land covers was circumvented by either removal of sites in the most egregious cases or adjustment of the assessment location to an area as close as possible to the water-level recording location but within marsh exhibiting the needed extent and uniformity.

Validating SAR Areal Data with Hydrologic Point Data

In the eastern coastal zone, where scattered pockets of persistent flooding commonly occurred, there was divergence between hydrologic data and SAR-based inundation detection (e.g., Ramsey, 1995).

Although hydrologic data indicated an increase in inundation surrounding data stations, in some cases the SAR data did not indicate that flooding encompassed the station itself. Such divergences lowered the performance success of SAR-based inundation mapping when compared to site-specific measurements of flood occurrences.

In this case, the comparability of SAR-based inundation products that are composites of spatially integrated ground elements (pixels of 100 and 150 m in this case) with point measurements (water-level recorder locations) was an issue (e.g., Fisher *et al.*, 2006; Fisher and Mustard, 2007). This incompatibility particularly in highly dynamic situations occurring in heterogeneous coastal environments may diminish the reliability of the assessment method. Alternatively, accurate determination of surface flooding, particularly when surface water levels are low (i.e., <10 cm), requires highly accurate ground-surface and water-level elevations and precisely functioning

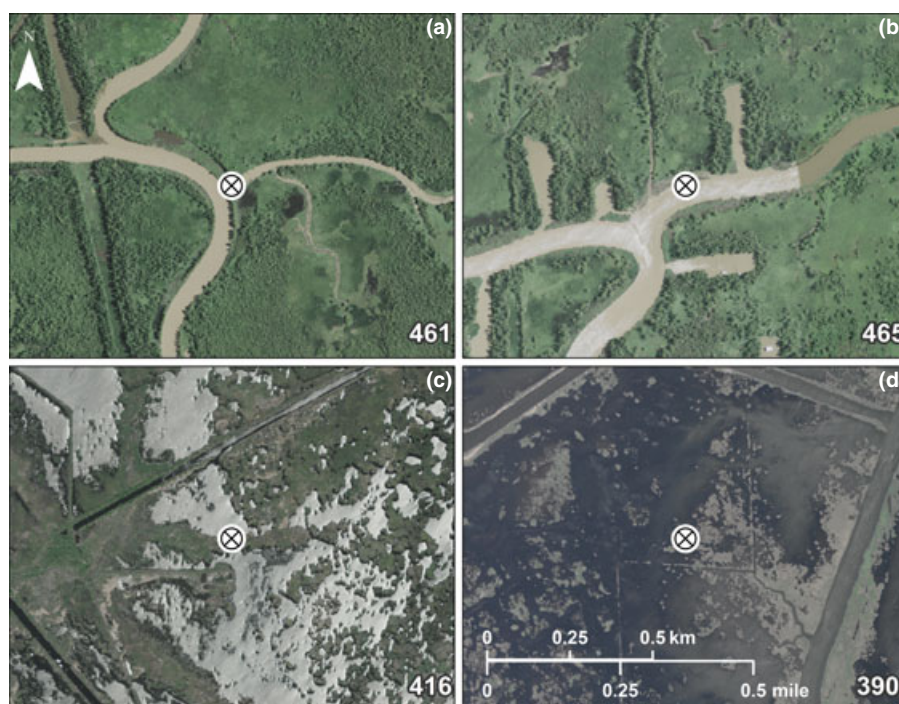


FIGURE 4. Examples of CRMS Inland Hydrologic Stations (solid white circles with X) for Which Data Were Unsuitable for Use as SAR-Based Inundation Reference Data. (a, b) Forests and shrubs within a marsh area at stations 461 and 465. (c, d) Degraded and predominantly open-water marsh that included stations 416 and 390.

water-level recorders. Inaccuracies in above-surface flood determination may also limit the validity of the point measurements, and in turn, decrease the perceived reliability of the SAR-based inundation products. To help improve the calibration and validation of the inundation maps by using inland water-level recordings, we inspected marsh areas adjacent to and surrounding hydrologic stations. These searches were limited to a 100-m (for PALSAR data) or 150-m (for ASAR data) radius surrounding hydrologic stations, within nominal ground resolutions. If there were flood occurrences within the pertinent 100- or 150-m radius, we concluded that the site was flooded.

Mapping Inundation Extent

Delineating Permanent Water Bodies. To minimize confusion among wind-roughened water surfaces, flooded marsh, and non-flooded marsh, permanent water bodies were defined within the study area (Ramsey *et al.*, 1994, 2011, 2012). The location and extent of permanent inland coastal waters obtained from the Louisiana Oil Spill Coordinator's Office (LOSCO) (LOSCO, 2007) were updated with 13 TM images collected from 2006 to 2008 before Hurricane Gustav (landfall September 1, 2008) (western region: June 4, 2006; April 20, August 10, and August 26, 2007; February 18, March 5, and July 27, 2008;

central region: June 13, 2006; April 29, 2007; and June 18, 2008; eastern region: June 6, 2006; April 6, 2007; and July 13, 2008). These TM images were registered to the same LCC-projected TM-base image used to register SAR scenes. LOSCO open-water coverage was superimposed on the suite of TM images, and the areas of omission in the LOSCO coverage compared to water bodies exhibited on the TM images were determined. To be retained, the initially omitted water bodies had to be at least 40 km² in area and exhibit spatial and temporal consistency throughout 2006 and 2008. Water bodies meeting these criteria were added to the LOSCO open-water polygon coverage. The combined water polygon coverage was used to exclude all permanent water bodies from the SAR-based change-detection products. In addition, a coastal extent vector was used to exclude offshore waters (LOSCO, 2007). Although alignment was present along most of the coast, location errors in the coastal vector were found in rapidly changing and spatially complex deltaic marshes, such as in the bird's foot of the Mississippi River Delta, the Atchafalaya Delta, and the Wax Lake Delta (Figure 1).

SAR Reference Scenes. To detect changes related to flooded marsh, each SAR scene was paired with a reference scene having the same HH or VV polarization to eliminate change artifacts associated with polarization differences. To successfully detect

changes related to subcanopy flooding, preferred reference scenes were those wherein there was no flooding and ponding present (Ramsey *et al.*, 2011, 2012). Choice of reference scene was intended to avoid collection times closely following rain events, high tides (spring tides), and atypically elevated sea levels (e.g., Figure 5); furthermore, reference scenes were chosen to reflect the lowest mean sea levels registered in data from NOAA coastal stations (Figures 1 and 6). These criteria for reference-scene selection helped insure that the change-detection method best captured subcanopy flooding.

Inundation Detection. To provide adequate inundation delineation, calibrated SAR scenes were subjected to a change-detection algorithm that compared the backscatter intensity of a target scene to that of its reference scene. The change-detection algorithm incorporated an internal 5-by-5 pixel Kuan speckle filter to dampen noise while preserving edges and shape (PCI Geomatics, 2007; Ramsey *et al.*, 2011, 2012). A logarithmic ratio resulting in a positive decibel difference (lower intensities in the target scene than in the reference scene) indicated possible inundation. To help alleviate change artifacts not related to inundation occurrences, minimum change thresholds were applied.

The image processing procedure used to determine the minimum acceptable change-detection threshold relied on an experienced operator intervention and judgment (Ramsey *et al.*, 2011, 2012). In principle, this required consideration of radar parameters for imaging flooded and non-flooded landscapes as well as background knowledge of flood condition and behavior

within a specific geographic setting; both aspects were considered in an informed trial-and-error procedure to determine the extent and configuration of flooded *vs.* non-flooded boundary lines. Threshold flood extent was evaluated for consistency by comparing results

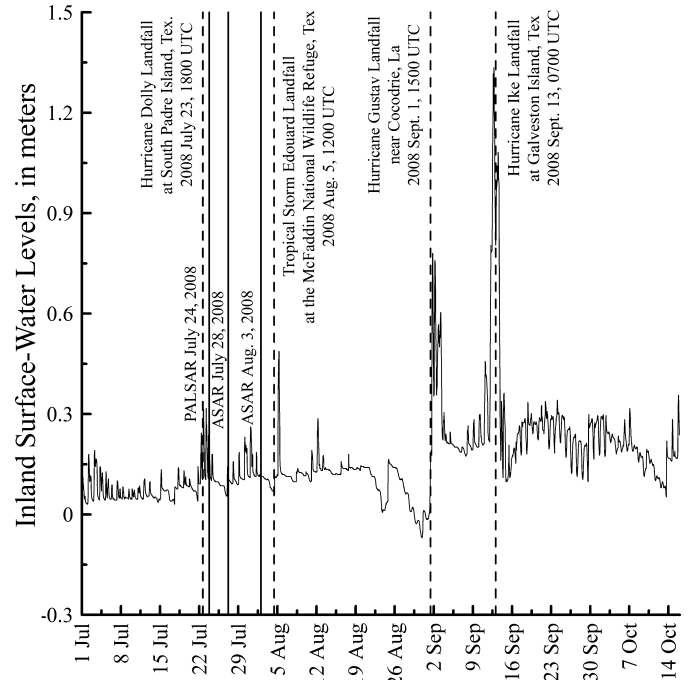


FIGURE 5. An Example of Water-Level Data Used in Selecting SAR Reference Scenes (solid lines) for the Flood Inundation Analysis. Abnormally high sea levels were associated with the impacts of Hurricanes Gustav and Ike and also with the passages of Hurricane Dolly and Tropical Storm Edouard (dashed lines) in the Gulf of Mexico.

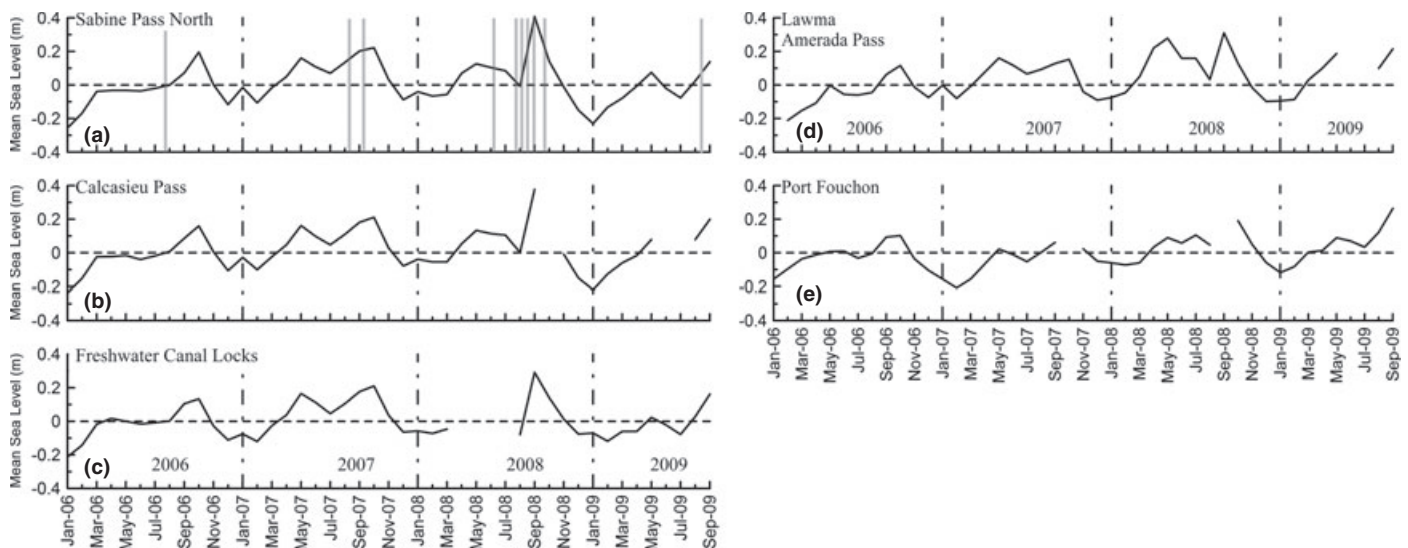


FIGURE 6. Monthly Mean Sea Levels from June 2006 to September 2009 at Coastal Hydrologic Stations (NOAA, 2010). (a) Sabine Pass North, (b) Calcasieu Pass, (c) Freshwater Canal Locks, (d) Lawma, Amerada Pass, and (e) Port Fourchon. Gray lines on (a) show dates of hurricanes or tropical storms in the Gulf of Mexico.

with the original SAR data, with the closest date of TM and inland water levels, and by categorizing landscape over a scene coverage by either over- or under-“saturating” it in such a way that known high ground was definitively excluded from contiguous “flooded” pixels and known low-lying flood-prone areas were included. Once appropriate threshold values were obtained, inundation extent along the entire Louisiana coast at the time of SAR collections was mapped.

RESULTS

Coastal and Inland Water Levels

Coastal Water Levels. All five NOAA coastal hydrologic stations recorded high variability in sea levels from east to west along the Louisiana coast (Figures 6a-6e). Many instances of elevated sea levels were associated with the passage of and impacts from tropical storms and hurricanes that occurred in the GOM from January 2006 to January 2010. Elevated sea levels prevalent in 2007 and 2008 were more prominent in the east than in the west. The consistency of elevated sea levels in 2007 and 2008, particularly in the spring to fall months, increased the difficulty in selecting reference SAR scenes that did not exhibit surface flooding or ponding.

Inland Water Levels. Of the 212 inland hydrologic stations, 67 were found acceptable for validation of the SAR-based inundation maps, most were in estuarine marshes. Of these, we used 14 stations located in the eastern region and 12 located in the western region (Figure 7). The selected stations were associated with comparatively consistent and reliable hydrographic records and were fairly well distributed across the coast at locations near to reasonably contiguous marsh where there were not numerous trees or shrubs.

Although they provided a good validation set, these stations and the associated water-level records were not without problems (e.g., Figure 4). Even so, the occurrence or absence of elevated water levels at the selected hydrologic stations provided an indication of flooding in the surrounding marshes, and thus, a reasonable measure of the performance of SAR-based flood detection.

Inundation Extent Mapping

PALSAR and ASAR Scene Collections. The look and orbit directions were nearly constant for all PALSAR scenes (Figure 3a). In contrast, the ASAR

scenes exhibited a high variety of orbit and look directions and thereby, highly variable coverages and orientations (Figures 3b and 3c). Also, the ASAR scenes exhibited a noticeably higher intensity difference from the near-range to the far-range and progressive decrease between ranges than were shown on the PALSAR scenes. Finally, polarizations in the ASAR scenes varied between HH and VV, in contrast to the constant HH polarization of the PALSAR scenes. The high level of variability in coverage and orientation led to highly variable local-incident angles at equivalent locations from scene to scene. Altogether, these limitations impeded comparability of the ASAR scenes.

SAR Reference Scenes. There were complications in choosing SAR reference scenes that would avoid abnormally high sea levels, over-saturated marsh soils, and growth phenologies different from those of target SAR scenes. As noted, during the only two complete years of collections (2007 and 2008), there were frequent and long durations of high sea levels and coastal flooding. These and other complications related to high variability in scene orientations and coverages resulted in there being no ASAR scene that was ideal for use as a reference in the change-detection procedure.

After extended comparisons, the most consistent reference scene selection criterion was found to be the lowest coastal water levels at the highest number of stations within eastern and western regions (Figure 6). Another useful criterion was intended to align the phenology of vegetation in the reference scene with that displayed in the majority of target scenes having the same type of polarization and the same regional coverage (i.e., eastern *vs.* western region). A final selection criterion used inland water levels recorded at the time of pertinent scene (reference, target) collections (Tables 2-4).

The single case where inland water levels changed the reference scene selection based on coastal water levels entailed the March 11, 2009, reference scene selection. Secondary inspection of inland water levels in the eastern region indicated that consistently lower levels occurred seven to eight months prior to the March 11 collection. Consequently, the March 11, 2009, scene was replaced with the July 28, 2008, scene as the ASAR (VV) reference scene for the eastern region. The replacement improved the accuracy of inundation mapping from 14 to 50%.

SAR-Based Change-Detection Thresholds

Multiple change-detection thresholds were tested for each PALSAR and ASAR set of scenes (eastern and western regions). Common to all change-detection

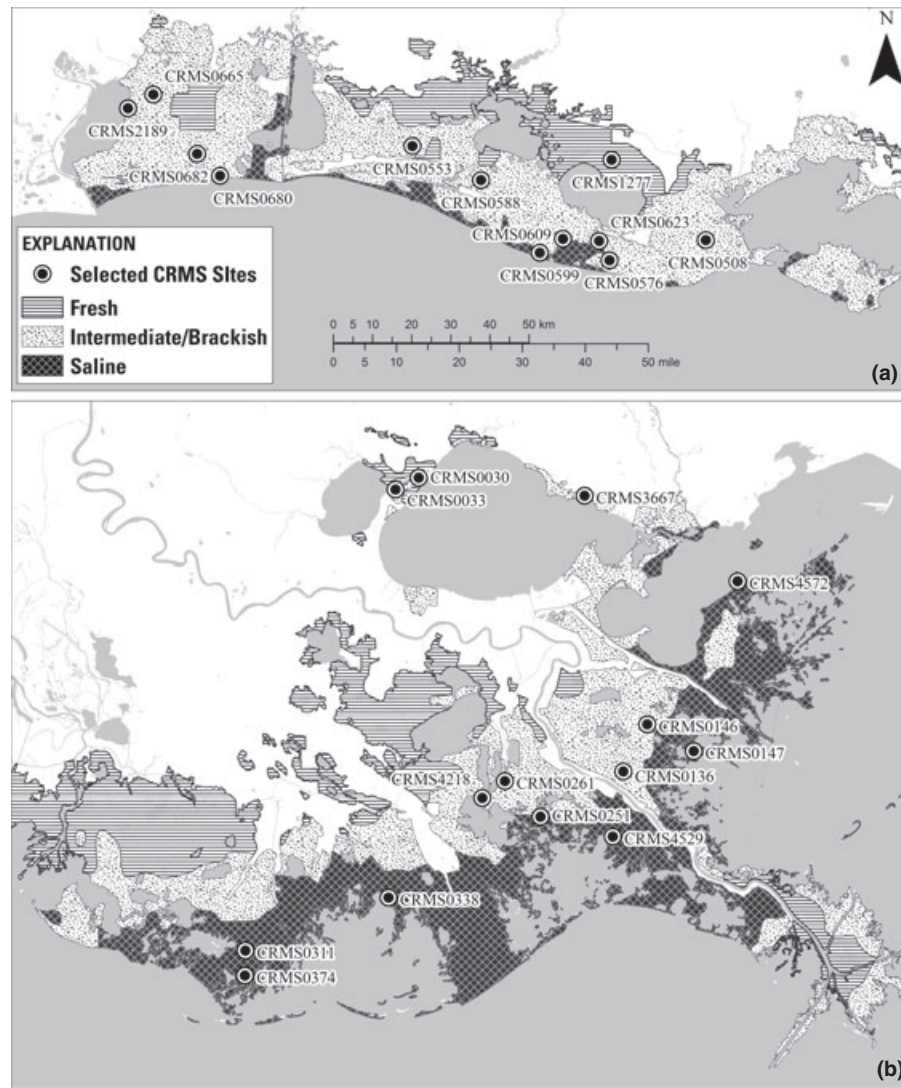


FIGURE 7. CRMS Hydrologic Stations in the (a) Western and (b) Eastern Regions of the Louisiana Coastal Zone. Estuarine marsh includes intermediate, brackish, and saline marshes. Selected CRMS sites were used in the validation of SAR-based inundation mapping.

algorithm products, the range and distribution of differences did not exhibit multimodal features but fairly continuous Gaussian-type distributions. This continuity has been noted and reported previously (Ramsey *et al.*, 2011, 2012). In the case of PALSAR scenes (all HH polarized), a threshold of 2 was chosen from results that included a range of threshold values from 1.5 to 2. For ASAR scenes, a threshold of 1 was selected for HH-polarized scenes, and threshold values of 0.5 (for the eastern region) and 1 (for the western region) were selected for VV-polarized scenes.

SAR-Based Inundation Maps

Inundation maps were produced by using calibrated SAR scenes (along with pertinent reference scenes) collected from 2006 to 2009 that were entered

into the change-detection procedure (Figures 8-10). PALSAR coverage in the eastern and the western coastal regions included a majority of scenes indicating extensive, contiguous areas of inundation *vs.* scenes with scattered inundation (Figures 8a and 8b).

Associated correspondence rates between inland water-level recordings and mapped inundations were 83% in the western region and 85% in the eastern region; rates ranged from 46 to 100% on any given date (Table 2a and b). In some cases, correspondence was decreased by surface water roughness of the surrounding inundated marshes (e.g., Ramsey *et al.*, 2009b; Figures 8a and 8b). More often, lower correspondence rates were associated with water levels near the ground surface (slightly above or below) (Table 2b). In particular, on July 24, 2008, the non-correspondence between mapped inundation and recorded below-surface water levels do not fit the

TABLE 2. Above-Ground Inland Water Levels (m) at CRMS Stations with ALOS PALSAR-Based (HH polarization) Flood Inundation Mapping Results. (a) Western and (b) eastern coastal Louisiana. White shows concurrence, black bold on black non-concurrence, and black bold on white reference.

Station ID	2008					2007					2009				
	January-7	February-22	July-10	August-25	October-10	November-25	January-10	July-24	September-8	October-15	November-30	January-17	January-12	September-16	
665	-0.250	-0.113	-0.021	0.152	0.104	-0.311	-0.317	0.006	0.091	NA	NA	0.149	NA	0.134	
311	-0.137	-0.030	0.180	0.283	0.180	-0.229	-0.192	0.140	0.241	0.351	-0.009	-0.101	-0.384	-0.140	
338	-0.168	-0.034	0.180	0.311	0.162	-0.250	-0.131	0.113	0.024	NA	NA	NA	NA	NA	
4218	NA	NA	NA	NA	NA	NA	NA	0.088	0.213	0.296	0.189	NA	NA	0.451	
261	NA	NA	0.061	0.162	0.171	-0.079	NA	0.128	0.250	0.283	0.198	NA	-0.256	0.363	
251	-0.018	-0.122	0.171	0.274	0.152	-0.113	-0.049	0.125	0.140	0.472	NA	-0.119	-0.238	0.390	
3667	NA	NA	NA	NA	0.207	0.091	0.006	NA	NA	0.472	0.012	0.027	NA	0.466	
30	NA	NA	-0.076	0.131	0.283	0.290	0.091	-0.046	0.351	0.448	0.055	NA	-0.140	0.268	
33	NA	NA	-0.177	0.058	0.305	0.122	0.015	-0.101	0.341	0.372	NA	-0.268	-0.003	0.396	
146	NA	NA	NA	NA	NA	0.238	-0.037	-0.064	0.317	0.427	NA	-0.119	-0.149	0.317	
136	-0.290	-0.402	-0.128	0.058	0.034	0.000	-0.320	-0.219	0.213	0.530	0.012	0.186	NA	0.226	
4529	NA	NA	NA	0.274	0.168	-0.247	-0.155	0.058	0.195	0.247	NA	NA	NA	0.475	
147	-0.326	-0.183	-0.009	0.256	0.216	-0.262	NA	-0.162	NA	0.433	NA	NA	-0.280	0.436	
4572	NA	NA	NA	NA	NA	0.098	-0.235	-0.070	NA	0.472	NA	NA	-0.287	0.494	

(a) Western Region

(b) Eastern Region

TABLE 3. Above-Ground Inland Water Levels (m) at CRMS Stations with ENVISAT ASAR-Based (HH polarization) Flood Inundation Mapping Results. (a) Western and (b) eastern coastal Louisiana. Cell highlighting as in Table 2.

(a) Western Region					
Station ID	2007	2006	2009		
	July-31	July-27	March-30	April-2	June-27
665	NA	NA	NA	0.162	-0.122
682	NA	NA	NA	-0.012	-0.247
588	0.088	NA	0.131	0.174	-0.052
599	-0.021	NA	0.055	0.134	-0.015
609	NA	NA	0.049	0.091	0.027
576	NA	NA	0.232	0.201	-0.055
508	NA	NA	0.137	0.131	-0.055
2189	0.079	NA	NA	0.204	NA
680	0.043	NA	NA	0.030	NA
553	0.326	NA	0.250	0.280	-0.012
623	NA	NA	0.171	0.183	-0.076
1277	NA	NA	0.128	0.119	-0.113

(b) Eastern Region				
Station ID	2009	2007	2009	
	March-30	July-25	June-24	June-27
374	NA	-0.079	NA	NA
311	-0.198	-0.052	-0.195	-0.034
338	-0.287	-0.027	-0.320	-0.082
4218	0.006	NA	-0.094	0.04
261	0.064	-0.116	0.003	0.131
251	-0.091	-0.07	-0.094	0.098
3667	0.168	NA	-0.250	-0.165
30	0.125	0.052	-0.128	0.101
33	0.259	0.009	-0.259	-0.067
146	-0.061	NA	NA	NA
136	-0.134	-0.396	-0.445	-0.226
4529	-0.274	NA	-0.235	0
147	-0.344	-0.192	NA	NA
4572	-0.18	NA	-0.329	-0.04

recorded surface flooding pattern to the west and inland (Table 2b) and generally higher coastal water heights during this period (Figure 6e). Overall, however, PALSAR-based (HH polarization) inundation mapping performed exceedingly well.

In contrast, most ASAR scenes displayed limited and scattered inundations in both coastal regions (Figures 9a, 9b, 10a, and 10b). For the western region, ASAR-based (HH polarization) mapping resulted in a 53% concurrence with inland water-level records (Table 3a; Figure 9a). In the eastern region the overall correspondence rate was 81% (Table 3b); however, the three ASAR scenes (HH polarization) comprising the eastern set (Figure 9b) were collected at times when marsh-surface inundation was mostly absent throughout the region.

With VV polarization, ASAR-based mapping of inundation in the western region exhibited an overall correspondence rate of 61%, which was primarily due to high correspondence for the September 14, 2008,

scene collected a short time after high surge levels, and spatially extensive flooding that occurred on August 3, 2008 (Ramsey *et al.*, 2009b) (Table 4a; Figure 10a). On the other hand, correspondence rates with inland water levels associated with the September 1, 2008, May 20 and 23, 2009, target scenes were extremely low (<50%) even though both May scenes were collected only days after the May 17, 2009, reference scene. On the May 20 and especially the September 1 and May 23 scenes backscatter was higher than on the reference scene. The higher backscatter in the target scenes, most likely resulting from differences in reference and target local incident angles, degraded the inundation mapping performance based on change detection. In addition, although high water-levels on September 14, 2008, a day after Hurricane Ike landfall enhanced ASAR inundation mapping performance overall, two locations (Table 4a) were misclassified as not flooded due to wind roughening of flood water overtopping the marsh.

TABLE 4. Above-Ground Inland Water Levels (m) at CRMS Stations with ENVISAT ASAR-Based (VV polarization) Flood Inundation Mapping Results. (a) Western and (b) eastern coastal Louisiana. Cell highlighting as in Table 2. Italics denote roughened water surface and flood delay.

(a) Western Region

Station ID	2009	2007		2008			2009	
	May-17	September-4	August-3	September-1	September-14	May-20	May-23	
665	0.296	NA	0.158	0.162	1.548	0.302	0.113	
682	-0.064	NA	-0.140	0.034	<i>1.655</i>	-0.067	-0.061	
588	0.128	0.128	0.040	-0.034	1.180	0.091	0.107	
599	0.009	-0.024	NA	0.015	0.884	0.101	0.146	
609	-0.03	NA	-0.040	-0.113	1.152	0.018	0.049	
576	0.101	NA	0.052	0.070	1.189	0.064	0.113	
508	-0.131	NA	-0.064	-0.195	1.228	-0.006	0.037	
2189	0.085	0.040	0.037	-0.052	NA	0.055	0.104	
680	-0.043	0.027	NA	0.021	<i>1.679</i>	-0.061	-0.061	
553	0.354	0.302	0.271	0.280	1.628	0.317	0.287	
623	0.064	NA	0.000	-0.223	1.097	0.024	0.076	
1277	0.146	NA	-0.354	-0.213	<i>0.165</i>	0.104	0.098	

(b) Eastern Region

Station ID	2008	2007	2008			2009					
	July-28	September-14	August-29	September-1	September-17	March-11	May-20	May-23	May-27	August-30	September-2
374	-0.101	-0.049	-0.265	-0.006	0.137	-0.061	0.043	-0.052	NA	NA	NA
311	-0.055	0.146	-0.207	0.073	0.210	0.012	0.088	0.006	NA	NA	-0.140
338	-0.104	0.189	-0.216	-0.064	0.296	0.070	0.268	0.055	0.338	NA	NA
4218	-0.14	NA	-0.110	-0.021	0.207	0.034	-0.024	0.094	0.146	-0.006	-0.070
261	-0.076	0.195	-0.073	-0.018	0.250	0.030	-0.024	0.128	0.183	0.055	-0.015
251	-0.128	0.189	-0.140	-0.018	0.570	0.067	0.003	0.064	0.232	0.049	-0.079
3667	NA	NA	NA	NA	0.229	-0.076	0.259	0.418	0.101	0.076	0.012
30	-0.204	0.101	-0.027	0.204	0.351	-0.021	0.347	0.500	0.076	0.091	0.043
33	-0.143	0.104	-0.091	0.076	0.418	-0.070	0.290	0.399	0.177	0.088	0.027
146	-0.277	NA	-0.119	0.277	0.168	-0.119	0.192	0.405	NA	NA	NA
136	-0.564	-0.277	-0.411	0.454	0.283	-0.192	0.494	0.539	0.024	-0.354	-0.265
4529	-0.11	0.216	-0.210	-0.198	0.183	0.037	-0.034	-0.061	0.326	0.091	-0.094
147	-0.332	-0.079	-0.360	0.701	0.131	-0.094	0.091	0.180	0.094	NA	NA
4572	-0.305	NA	-0.351	0.375	0.241	-0.070	0.146	0.216	0.134	-0.192	-0.140

The second highest number of inundation maps was created from ASAR VV scenes covering the eastern region (Figure 10b). For this region, the overall correspondence rate with inland water levels was 61% with the lowest correspondence rates associated with the September 1 and 17, 2008 (<42%), scenes closely followed by September 14, 2007 (50%), and those associated with March 11, and May 20 and 23, 2009, scenes (<57%) (Table 4b). Although some blurring of the backscatter along the coastal shore as obvious in the western September 14, 2008, scene (Figure 10a) may have influenced the mapping performance in certain cases, near-range brightening was evident in four of the scenes associated with the worst inundation mapping performance. The highest per scene correspondences were associated with August 29, 2008, scene. At all but one hydrographic station on August 29, however, water levels were

recorded well below the ground surface. Also noticeable was a pattern of correspondence with marsh type in the eastern ASAR VV scene coverages. Inundation correspondence with water levels located in intermediate marshes averaged 74% ($n = 62$) while correspondence in saline marshes averaged 46% ($n = 61$) (Figure 7b).

DISCUSSION

Performance of PALSAR- and ASAR-Based Inundation Mapping

Even though no PALSAR and ASAR scenes were collected on the same day, comparing differences in

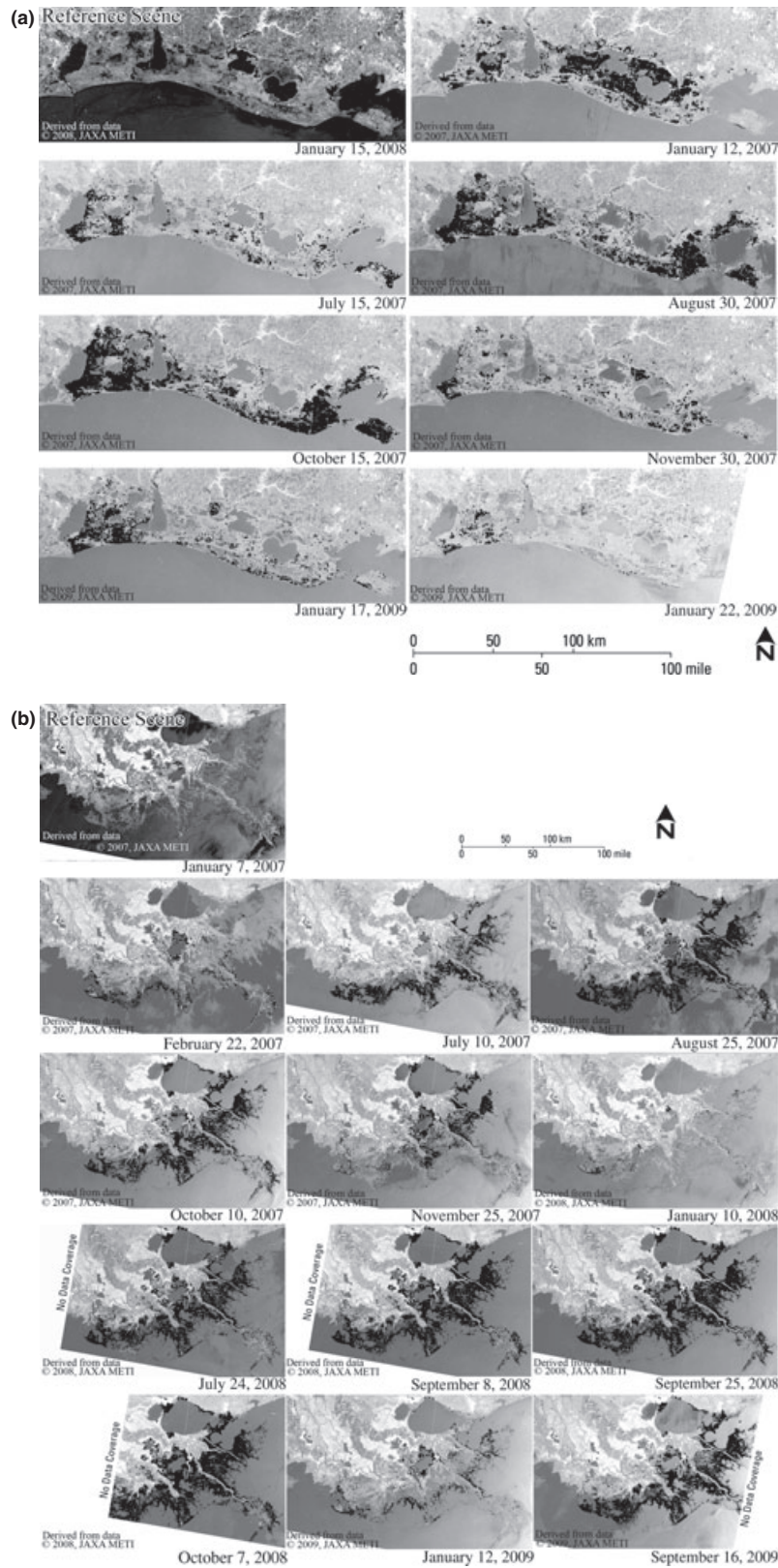


FIGURE 8. (a) Western ALOS PALSAR-Based Flood Inundation Results with Sigma-Naught Coefficient (σ_0) Scaled in Decibels. For clarity, target scene contrast is subdued relative to the reference scene (upper left) to highlight flood inundation depicted in solid black. (b) Eastern ALOS PALSAR-based flood inundation results with sigma-naught coefficient (σ_0) scaled in decibels. Highlighting as in Figure 8a.

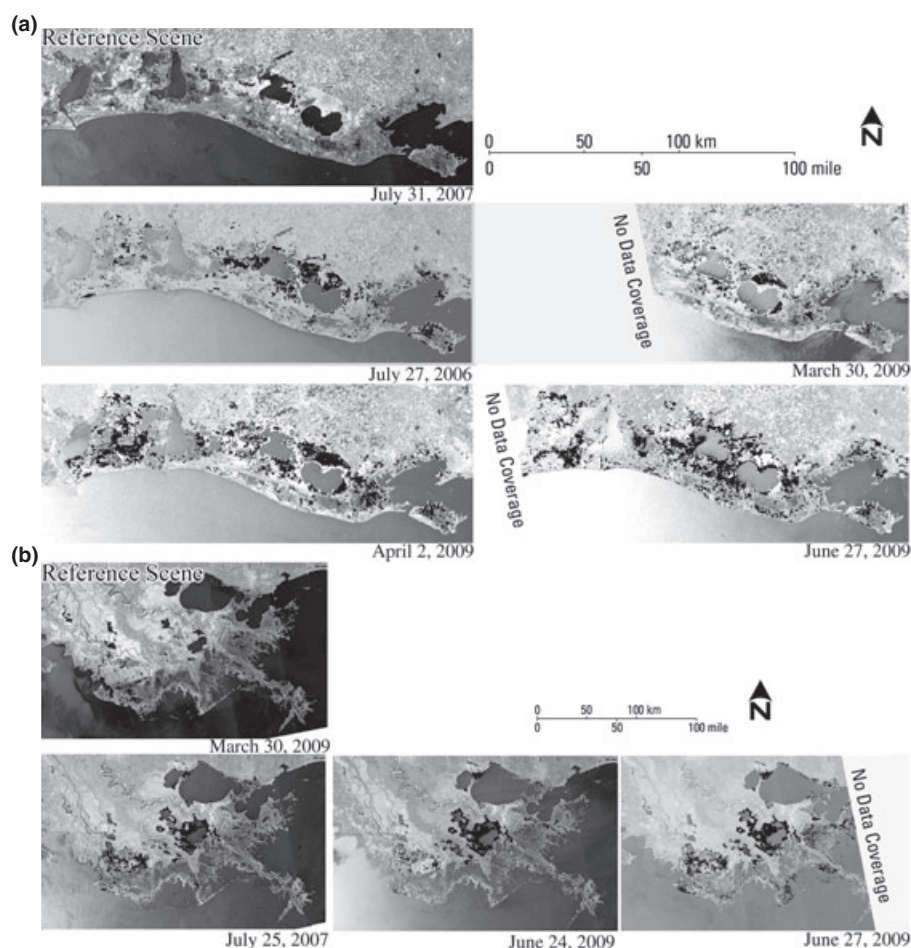


FIGURE 9. (a) Western and (b) Eastern ENVISAT ASAR HH-Based Flood Inundation Results with Sigma-Naught Coefficient (σ_0) Scaled in Decibels. Highlighting as in Figure 8a.

inundation extensiveness and contiguousness associated with the two sensors on dates within close proximity offers insight into their respective mapping effectiveness. At the time of the eastern August 29, 2008, ASAR (VV) scene collection when inland surface-water depths averaged -21 cm (Table 4b) mapped surface inundation was limited to the furthest ocean extent of the Mississippi River Delta. In comparison, inundation which was fairly extensive (24 cm average depth, Table 2b) on the September 8, 2008, PALSAR scene, changed little (38 cm average depth, Table 2b) by the time the September 25, 2008, PALSAR scene was acquired. In this comparison, the difference between PALSAR- and ASAR-based inundation maps was related to differences in water levels. However, at the time of the September 17, 2008, ASAR scene collection when inland water depths averaged 26 cm (Table 4b), inundation was only somewhat more extensive than that depicted on the August 29 ASAR scene.

A possible explanation for the high disparity between the ASAR- and PALSAR-based inundation

extent when average water depths at the time of the ASAR collection fell in between the 24 cm and 37 cm associated with the two PALSAR collections is an overemphasis of inundation associated with PALSAR data. However, outside the low performance results associated with the July 24, 2008, scene possibly related to residual ponded water and over-saturated soils (e.g., Ramsey, 1995; Ramsey *et al.*, 2006), inspection of eastern PALSAR inundation maps showed that low or below-surface inland water levels were associated with a paucity of inundation occurrences similar to that exhibited on the August 29 ASAR-based inundation map (e.g., see data for January 7, 2007, January 10, 2008, and January 12, 2009, in Figure 8b).

Finally, the discrepancy between the ASAR- and PALSAR-based inundation maps could be related to accuracy. Binomial comparisons, however, indicated that correspondence rates between mapped inundations and inland water levels were higher with PALSAR and lower with ASAR. In this instance, ASAR-based change detection failed to provide spatial

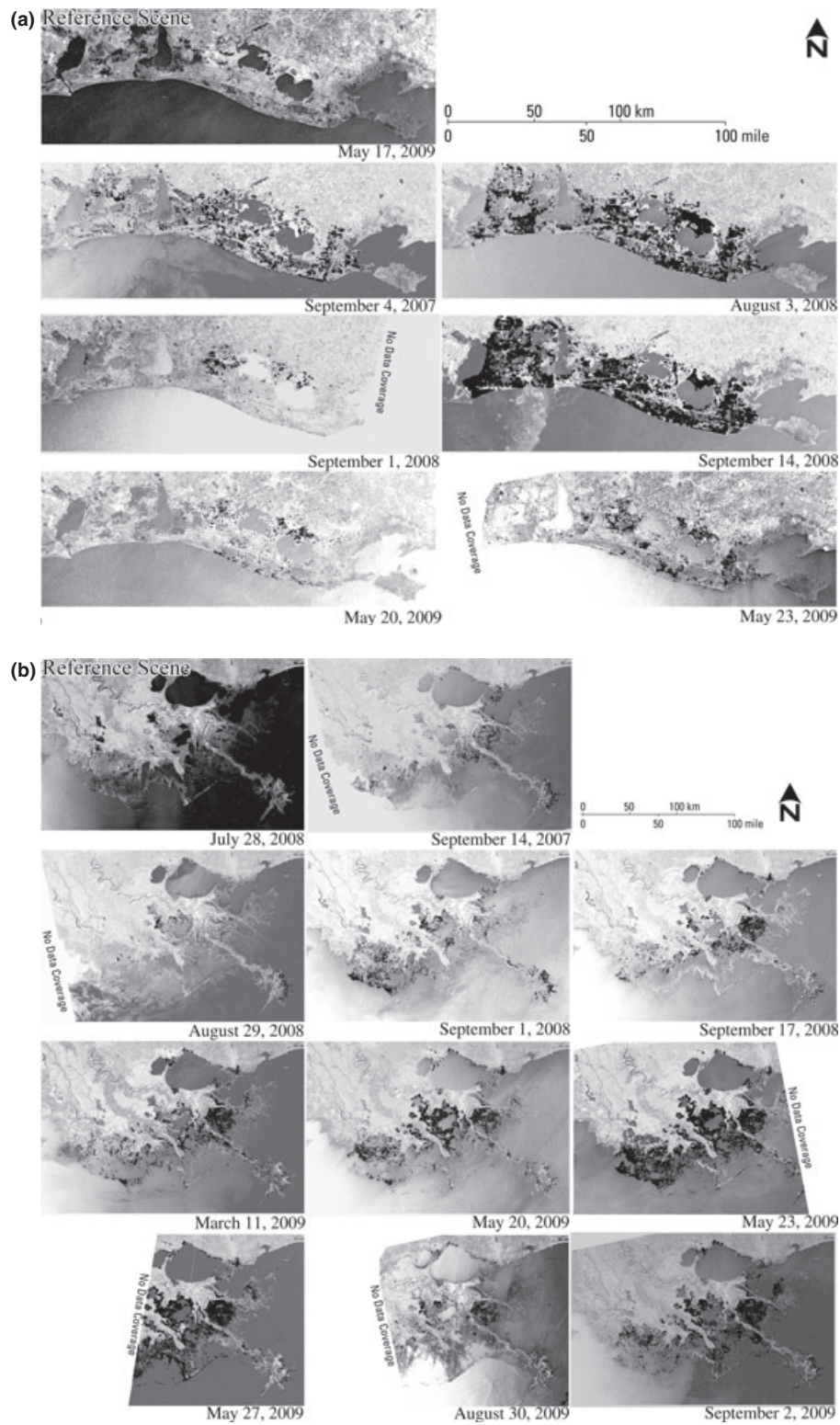


FIGURE 10. (a) Western ENVISAT ASAR VV-Based Flood Inundation Results with Sigma-Naught Coefficient (σ_0) Scaled in Decibels. Highlighting as in Figure 8a. (b) Eastern ENVISAT ASAR VV-based flood inundation results with sigma-naught coefficient (σ_0) scaled in decibels. Highlighting as in Figure 8a.

inundation patterns that were consistent with the inland surface-water levels and comparable with the more reasonable and internally consistent PALSAR-based inundation patterns.

Complications of ASAR-Based Inundation Mapping

Complications in the inundation mapping with ASAR to some extent stemmed from a lack of high-quality ASAR reference scenes resulting from the abnormally high sea levels in 2007 and 2008. High coverage variability also hindered conformity between ASAR reference and target scenes, whereas collection parameters of all PALSAR scenes were similar from scene to scene. ASAR scenes also exhibited a pronounced drop off in brightness from near-to-far range that was not visible in the PALSAR scenes.

The reason for the progressive change in backscatter with look angle could be related in part to the nearly flat GOM coastal landscapes that support marshes exhibiting an overall more vertical orientation (Ramsey *et al.*, 1999, 2004). In this case, increases in the look angle (from near-to-far range) would tend to increase canopy interaction and decrease surface backscatter (Ramsey, 1998). In addition to the more direct surface-scatter return of the more vertical look angle, the prominence of moist soils in such wetland environments further enhances backscatter. Although the incident SAR is, for the most part, reflected away from the sensor when conditions are at and above soil saturation, thus decreasing the response (Chanzy, 1993; Ramsey, 1998), soil moisture up to saturation enhances scatter (Chanzy, 1993; Kasischke *et al.*, 2003). In this case, the higher the canopy penetration, the more likely an enhanced backscatter. The progressive decrease in penetration is exhibited as a progressive decrease in backscatter or brightening from near-to-far range.

Quantitative assessment linking the performance of ASAR-based mapping to look angle was not performed; however, the lower coverage extent and orientation comparability between ASAR scenes limited the ASAR-based inundation mapping performance. Even though variability in the reference and target scene look directions might not have substantially influenced inundation mapping performance, the variable look directions and accompanying coverage footprints combined with the pronounced change in backscatter from near to far range compounded differences at equivalent locations on the reference and target ASAR scenes, especially in the near range. These variations were not present or less severe in the temporal set of PALSAR scenes resulting in a higher comparability between reference and target PALSAR scenes than obtainable within the set of

available ASAR scenes. The lower ASAR reference and target scene comparability degraded the ASAR-based inundation mapping performance.

The dominantly vertically oriented marsh structures could have also selectively influenced performance of the SAR-based inundation maps with respect to polarization (Ramsey *et al.*, 2004, 2009a). While vertical polarizations would be more prone to interact with marsh canopy, horizontal polarizations would tend to penetrate further into the subcanopy (Elachi, 1988; Ramsey, 1998; Ramsey *et al.*, 1999), and thus, to provide more consistent detection of subcanopy inundation. Although this preferential canopy penetration of horizontal polarizations has been demonstrated (Ramsey *et al.*, 1999), there was no indication of improved inundation mapping performance associated with HH-polarized ASAR than VV-polarized ASAR. Similarly, even though HH polarization exhibits lower sensitivity than VV to enhanced backscatter from roughened water surfaces (Henry *et al.*, 2006; Matgen *et al.*, 2007) this dichotomy was not apparent in the current study. Of the two operational parameters, local incident angle variability had a more noticeable effect on ASAR-based inundation mapping performance than did polarization.

Finally, even though the study objective did not include segmentation by marsh class, we noted that ASAR-based inundation mapping accuracy exhibited a possible spatial correspondence with marsh class. This correspondence suggests higher inundation performance in intermediate-brackish than saline estuarine marshes in eastern Louisiana. Although temporal observations were more limited, a similar pattern was noticed in Ramsey *et al.* (2012). In that study, the change in canopy structure accompanying the change in dominant species comprising the two marshes was suggested to differentially retard radar penetration into the saline marsh subcanopy, and thus, lower inundation performance in the eastern saline *vs.* intermediate-brackish marshes. Even though the canopy structure association with ASAR-based performance is inferential, the results of this study support the assertion of a canopy structure influence on flood inundation mapping in eastern Louisiana coastal marshes.

Extending the Binomial Presence and Absence Comparisons

Although water levels were not directly mapped, water levels recorded at inland hydrologic stations elucidated the variable performance of SAR-based inundation mapping. In GOM marshes, previous studies have demonstrated a decrease in SAR backscatter with increasing flood depth (Kasischke *et al.*,

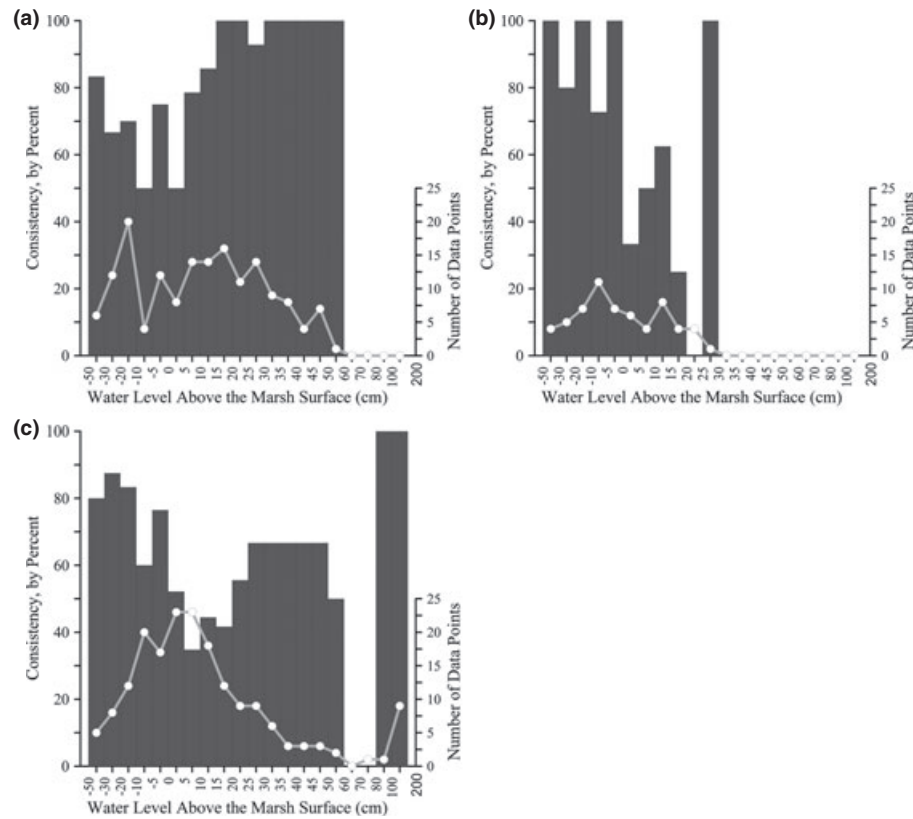


FIGURE 11. The Percent Correspondence (vertical bars) between the Presence or Absence of Surface Water at Inland Hydrographs and SAR-Based Flood Inundation Mapping *vs.* Co-occurring Measured Water Levels Partitioned into 5 cm or 10 cm Depth Increments (horizontal axis). (a) PALSAR, (b) ASAR HH, (c) ASAR VV. The dots on the solid white line denote the number of observations per depth increment used in the percent correspondence calculation.

2003). Results have also confirmed that SAR backscatter can increase with increasing marsh biomass when flooded and decrease with increasing biomass when not flooded (Dobson *et al.*, 1996). The decrease in backscatter associated with non-flooded marsh may be linked to a loss of enhanced backscatter from underlying moist soils. These results are expected to differ when using L-band *vs.* C-band SAR systems because of the higher marsh-penetration potential of the former (Ramsey, 1998, 2005; Ramsey *et al.*, 2011).

To include water-depth information in the SAR-based inundation analyses, correspondence rates between inland water levels and the inundation maps (aggregated per PALSAR and ASAR [HH or VV polarized] sensor) were graphically portrayed (Figures 11a-11c). High rates of correspondence between PALSAR-mapped inundations and inland water levels are shown in Figure 11a, which also shows how correspondence rates vary with water depths. The high rates of correspondence also agree with the conformity of spatial inundation exhibited on the PALSAR-based maps. In addition, the correspondence rates and water-level distribution depicts possible

limitations in the inundation mapping. In general, as water levels became shallower (<5 cm), correspondence rates associated with PALSAR-based mapping decreased ($\approx 50\%$) until water levels were further below the marsh surface (≤ -10 cm).

Both HH and VV ASAR-based mapping depict similar results in the correspondence and depth bar plots (Figures 11b and 11c); however, the VV ASAR-based mapping plot is more fully populated (Figure 11c). With ASAR-based mapping, correspondence rates decreased below 40% when water levels were close to the surface and increased to above 60-80% when water levels were far below or far above the ground surface.

In both PALSAR-based and ASAR-based inundation mapping, near-surface water levels are potentially associated with increased ponding and at the same time enhanced backscatter caused by increased soil moisture up to saturation; both situations can decrease inundation mapping performance as evaluated by point measures of water level. In contrast to the PALSAR-based mapping, the lowest ASAR-based mapping accuracies occupied a broader range of shallow flood depths (<20 cm, VV ASAR) and were largely

associated with above surface water level recordings while the lowest PALSAR-based mapping accuracies were centered about the ground surface (± 5 cm). In both ASAR-based and PALSAR-based mapping, as the marsh dried out over a period of time, the conflicting influences on the backscatter diminished, resulting in improved mapping performance.

CONCLUSIONS

In this study, we demonstrated the ability to monitor the distribution and occurrence of inundation covering spatially extensive Louisiana coastal marshes. The strategy for detecting inundation was based on scenes collected during routine operations of the ALOS PALSAR L-band and ENVISAT ASAR C-band satellite sensor systems. To provide the highest available collection frequency and contiguous coverages, while retaining a workable ground spatial resolution, we used PALSAR Wide Beam (100 m) and ASAR Wide Swath (150 m) image collection modes. Inundation mapping success was based on the level of correspondences between mapped inundation and inland water-level concurrences.

Although, the HH-polarized PALSAR (21 scenes), VV-polarized ASAR (17 scenes), and HH-polarized ASAR (7 scenes) collections did not allow for a fully strategic evaluation of mapping performance or the direct comparison of L- and C-band SAR effectiveness, the results presented in this study provide an appropriate indication of the baseline inundation mapping performance achievable based on current scene availability and provide several key findings. In contrast to L-band PALSAR-based mapping, C-band ASAR-based inundation mapping was beset with highly variable scene coverages and look directions, resulting in variable local incident angles from scene to scene. These variations combined with the progressive decrease in backscatter from near-to-far range exhibited in ASAR scenes, led to a higher likelihood that variable backscatter from date to date associated at the same physical location from scene to scene diminished the success of discerning the presence or absence of flood inundation.

In both the PALSAR- and ASAR-based inundation mapping, the binary comparisons indicated higher positive correspondences when water levels were either much higher or much lower than marsh-surface heights. These patterns tended to be more pronounced in the ASAR-based results and the lowered inundation mapping accuracies incorporated higher depths of surface flooding than exhibited in the PALSAR-based inundation mapping. In eastern

Louisiana ASAR-based inundation mapping, higher accuracies tended to be associated more with intermediate-brackish as compared to more coastal saline marshes. Overall, the binary assessment of PALSAR-based inundation averaged 84% ($n = 160$) indicating a consistent performance and overall high correspondence with inland water-level recordings accuracies. The ASAR-based inundation mapping accuracy averaged 62% ($n = 245$), increasing performance levels resulting when water levels were well below or above the ground surface extensively throughout the scene.

Our research suggests that although both PALSAR- and ASAR-based inundation mapping performance would benefit from higher frequency collections, ASAR-based performance would have a substantially higher improvement potential. In the case of ASAR in particular, a higher collection frequency would provide more choices leading to the possibility of obtaining consistently higher-quality reference scenes leading to improved inundation mapping performance. In addition, results suggest that the application of more consistent SAR imaging parameters, such as look direction and coverage would increase SAR inundation mapping performance, primarily by increasing the consistency in look angle from scene to scene. With these strategic collection changes, SAR inundation mapping could provide an improved representation of the coastal flooding dynamism.

ACKNOWLEDGMENTS

ENVISAT ASAR data are copyrighted by the ESA and were provided via the Cat-1 2853 and 7286 Projects. The ALOS PALSAR data (©2007, ©2008, ©2009, JAXA METI) were provided by the University of Alaska and National Aeronautics & Space Administration (NASA) Alaska Satellite Facility. This research contributed to the study "Monitoring Coastal Marshes for Persistent Flooding and Salinity Stress" (Principal Investigator Dr. Maria Kalcic) and was in part supported under the "Earth and Science for Decision Making: GOM Region" program (NNH08ZDA001N-GULF). We thank Dr. Anthony Filippi and Dr. Charles Bachmann for their thoughtful reviews. Also, we are grateful for the technical editing done by the USGS Lafayette Publishing Service Center. This work was funded entirely by the United States Federal Government and performed by Federal employees and employees of Five Rivers Services, LLC under contract no. G11PC00013 with the Federal Government. Any use of trade, product, or firm names is for descriptive purposes only and does not imply endorsement by the U.S. Government.

LITERATURE CITED

Chabreck, R., 1970. Marsh Zones and Vegetative Types in the Louisiana Coastal Marshes. Ph.D. Dissertation, Louisiana State University (LSU), Baton Rouge, Louisiana.

- Chanzy, A., 1993. Basic Soil Surface Characteristics Derived from Active Microwave Remote Sensing. *Remote Sensing Reviews* 7 (3):303-319.
- Dobson, M., L. Pierce, and F. Ulaby, 1996. Knowledge-Based Land-Cover Classification Using ERS-1/JERS-1 SAR Composites. *IEEE Transactions on Geoscience and Remote Sensing* 34(1):83-99.
- Elachi, C., 1988. *Spaceborne Radar Remote Sensing: Applications and Techniques*. IEEE Press, New York City, New York.
- ESA (European Space Agency), 2007. Envisat ASAR Product Handbook, Issue 2.2. <http://Envisat.esa.int/handbooks/asar/>, accessed July 2011.
- Fisher, J. and J. Mustard, 2007. Cross-Scalar Satellite Phenology from Ground, Landsat, and MODIS Data. *Remote Sensing of Environment* 109:261-273.
- Fisher, J., J. Mustard, and M. Vadeboncoeur, 2006. Green Leaf Phenology at Landsat Resolution: Scaling from the Field to the Satellite. *Remote Sensing of Environment* 100:265-279.
- Grings, F., P. Ferrazzoli, H. Karszenbaum, J. Tiffenberg, P. Kandus, L. Guerriero, and J. Jacobo-Berrles, 2005. Modeling Temporal Evolution of Junco Marshes Radar Signatures. *IEEE Transactions on Geoscience and Remote Sensing* 43(10):2238-2245.
- Hager, B., B. Brakenridge, J. Eichelberger, C. Hunsaker, T. Killen, L. Zhong, J. Parrish, B. Pichel, D. Turcotte, N. Woodward, C. Dobson, J. Sauber, M. Moghaddam, E. Ramsey, III, B. Holt, R. Blom, B. Huberty, M. Glasscoe, P. Clemente-Colón, and B. Brooks, 2009. Hydrological and Ocean Applications. *In: Report of the DESDynI Applications Workshop October 29-31, 2008, UC Sacramento Conference Center, National Aeronautics and Space Administration, Jet Propulsion Laboratory, California Institute of Technology, Pasadena, California*, pp. 33-56. http://desdyni.jpl.nasa.gov/files/DESDynI_Applications_Report_V1.0.pdf, accessed April 2013.
- Henry, J., P. Chastanet, K. Fellah, and Y. Desnos, 2006. Envisat Multi-Polarized ASAR Data for Flood Mapping. *International Journal of Remote Sensing* 27(10):1921-1929.
- Hess, L., J. Melack, S. Filoso, and Y. Wang, 1995. Delineation of Inundated Area and Vegetation Along the Amazon Floodplain with the SIR-C Synthetic Aperture Radar. *IEEE Transactions on Geoscience and Remote Sensing* 33(4):896-904.
- Hong, S., S. Wdowinski, and S. Kim, 2010. Evaluation of TerraSAR-X Observations for Wetland InSAR Application. *IEEE Transactions on Geoscience and Remote Sensing* 48(2):864-873.
- Horritt, M., D. Mason, and A. Luckman, 2001. Flood Boundary Delineation from Synthetic Aperture Radar Imagery Using a Statistical Active Contour Model. *International Journal of Remote Sensing* 22(13):2489-2507.
- Kasischke, E., K. Smith, L. Bourgeau-Chavez, E. Romanowicz, S. Brunzell, and C. Richardson, 2003. Effects of Seasonal Hydrologic Patterns in South Florida Wetlands on Radar Backscatter Measured from ERS-2 SAR Imagery. *Remote Sensing of Environment* 88:423-441.
- Kiage, L., N. Walker, S. Balasubramanian, A. Babin, and J. Barras, 2005. Applications of Radarsat-1 Synthetic Aperture Radar Imagery to Assess Hurricane-Related Flooding of Coastal Louisiana. *International Journal of Remote Sensing* 26(24):5359-5380.
- Klemas, V., 2005. Resolution Requirements for Coastal Applications of New Geostationary Satellites. *In: Balancing on the Edge: Coastal Zone '05, Proceedings of the 14th Biennial Coastal Zone Conference, National Oceanic and Atmospheric Administration Coastal Services Center, New Orleans, Louisiana*. https://www.csc.noaa.gov/cz/CZ05_Proceedings/pdf%20files/Klemas.pdf, accessed April 2013.
- Klemas, V., J. Dobson, R. Ferguson, and K. Haddad, 1993. A Coastal Land Cover Classification System for the NOAA Coastal Change Analysis Project. *Journal of Coastal Research* 9 (3):862-872.
- Lang, M., P. Townsend, and E. Kasischke, 2008. Influence of Incidence Angle on Detecting Flooded Forests Using C-HH Synthetic Aperture Radar Data. *Remote Sensing of Environment* 112:3898-3907.
- Lecote, R. and T. Pultz, 1991. Evaluation of the Potential of Radarsat for Flood Mapping Using Simulated Satellite SAR Imagery. *Canadian Journal of Remote Sensing* 17:241-249.
- Lewis, A., F. Henderson, and D. Holcomb, 1998. *Radar Fundamentals: The Geoscience Perspective*. *In: Principles and Applications of Imaging Radar, F. Henderson and A. Lewis (Editors)*. Wiley, New York City, New York, pp. 131-181.
- Louisiana Oil Spill Coordinator's Office (LOSCO), 2007. Louisiana GIS Digital Map. Digital Versatile Disc, Baton Rouge, Louisiana.
- Lu, Z. and O. Kwoun, 2008. Radarsat-1 and ERS Interferometric Analysis over Southeastern Coastal Louisiana: Implication for Mapping Water-Level Changes Beneath Swamp Forests. *IEEE Transactions on Geoscience and Remote Sensing* 46(4):2167-2184.
- Lunetta, R., J. Lyon, B. Guindon, and C. Elvidge, 1998. North American Landscape Characterization Dataset Development and Data Fusion Issues. *Photogrammetric Engineering & Remote Sensing* 64(8):821-829.
- Matgen, P., G. Schumann, J. Henry, L. Hoffmann, and L. Pfister, 2007. Integration of SAR-Derived River Inundation Areas, High-Precision Topographic Data and a River Flow Model Toward Near Real-Time Flood Management. *International Journal of Applied Earth Observation and Geoinformation* 9:247-263.
- Moghaddam, M., K. McDonald, J. Cihlar, and W. Chen, 2003. Mapping Wetlands of North American Boreal Zone from Satellite Radar Imagery. *In: Proceedings of the Geoscience and Remote Sensing Symposium, IGARSS '03, Toulouse, France*, pp. 261-263.
- Morton, R., J. Bernier, J. Barras, and N. Ferina, 2005. Rapid Subsidence and Historical Wetland Loss in the Mississippi Delta Plain: Likely Causes and Future Implications, U.S. Geological Survey Open-File Report 2005-1216. <http://pubs.usgs.gov/of/2005/1216>, accessed July 2011.
- Neyland, R., 2007. The Effects of Hurricane Rita on the Aquatic Vascular Flora in a Large Fresh-Water Marsh in Cameron Parish, Louisiana. *CASTANEA* 72(1):1-7.
- Nielsen, C. and D. Werle, 1993. Do Long-Term Space Plans Meet the Needs of the Mission to Planet Earth? *Space Policy* 9(1):11-16.
- NOAA (National Oceanic and Atmospheric Administration), 2010. NOAA Tides and Currents Center for Operational Oceanographic Products and Services, U.S. Department of Commerce, NOAA National Ocean Service. <http://tidesandcurrents.noaa.gov/index.shtml>, accessed September 2010.
- Ormsby, J., B. Blanchard, and A. Blanchard, 1985. Detection of Lowland Flooding Using Active Microwave Systems. *Photogrammetric Engineering & Remote Sensing* 51:317-328.
- PCI Geomatics, 2007. *Geomatica User Guide*. PCI Geomatics Enterprises Inc., Richmond Hill, Ontario, Canada.
- Pope, K., E. Rejmankova, J. Paris, and R. Woodruff, 1997. Detecting Seasonal Flooding Cycles in Marshes of the Yucatan Peninsula with SIR-C Polarimetric Radar Imagery. *Remote Sensing of Environment* 59:157-166.
- Ramsey, III, E., 1995. Monitoring Flooding in Coastal Wetlands by Using Radar Imagery and Ground-Based Measurements. *International Journal of Remote Sensing* 16:2495-2502.
- Ramsey, III, E., 1998. Radar Remote Sensing of Wetlands. *In: Remote Sensing Change Detection: Environmental Monitoring*

- Methods and Applications, R. Lunetta and C. Elvidge (Editors). Ann Arbor Press, Inc., Ann Arbor, Michigan, pp. 211-243.
- Ramsey, III, E., 2005. Remote Sensing of Coastal Environments. *In: Encyclopedia of Coastal Science, Encyclopedia of Earth Sciences Series*, M.L. Schwartz (Editor). Kluwer Academic Publishers, Dordrecht, The Netherlands, pp. 797-803.
- Ramsey, III, E., S. Laine, D. Werle, B. Tittley, and D. Lapp, 1994. Monitoring Hurricane Andrew Damage and Recovery of the Coastal Louisiana Marsh Using Satellite Remote Sensing Data. *In: Proceedings of the Coastal Zone Canada '94*, P. Wells and P. Ricketts (Editors). Coastal Zone Canada Association, Dartmouth, Nova Scotia, pp. 1841-1852.
- Ramsey, III, E., Z. Lu, A. Rangoonwala, and R. Rykhus, 2006. Multiple Baseline Radar Interferometry Applied to Coastal Landcover Classification and Change Analyses. *GIScience & Remote Sensing*. 43(4):283-309.
- Ramsey, III, E., Z. Lu, Y. Suzuoki, A. Rangoonwala, and D. Werle, 2011. Monitoring Duration and Extent of Storm Surge Flooding Along the Louisiana Coast with Envisat ASAR Data. *IEEE Transactions on Geoscience and Remote Sensing* 4(2):387-399.
- Ramsey, III, E., G. Nelson, F. Baarnes, and R. Spell, 2004. Light Attenuation Profiling as an Indicator of Structural Changes in Coastal Marshes. *In: Remote Sensing and GIS Accuracy Assessment*, R. Lunetta and J. Lyon (Editors). CRC Press, New York City, New York, pp. 59-73.
- Ramsey, III, E., G. Nelson, S. Laine, W. Topham, and R. Kirkman, 1998. Generation of Coastal Marsh Topography with Radar and Ground-Based Measurements. *Journal of Coastal Research* 14(3):1158-1164.
- Ramsey, III, E., G. Nelson, S. Sapkota, S. Laine, J. Verdi, and S. Krasznay, 1999. Using Multiple Polarization L Band Radar to Monitor Marsh Burn Recovery. *IEEE Transactions on Geoscience and Remote Sensing* 37(1):635-639.
- Ramsey, III, E., III and A. Rangoonwala, 2006. Site-Specific Canopy Reflectance Related to Marsh Dieback Onset and Progression in Coastal Louisiana. *Photogrammetric Engineering and Remote Sensing* 72(6):641-652.
- Ramsey, III, E., A. Rangoonwala, F. Baarnes, and R. Spell, 2009a. Mapping Fire Scars and Marsh Recovery with Remote Sensing Image Data. *In: Remote Sensing and GIS for Coastal Ecosystem Assessment and Management*, X. Yang (Editor). Springer Lecture Notes in Geoinformation and Cartography, Berlin, Germany, pp. 415-438.
- Ramsey, III, E., D. Werle, Z. Lu, A. Rangoonwala, and Y. Suzuoki, 2009b. A Case of Timely Satellite Image Acquisitions in Support of Coastal Emergency Environmental Response Management. *Journal of Coastal Research* 25(5):1168-1172.
- Ramsey, III, E., D. Werle, Y. Suzuoki, A. Rangoonwala, and Z. Lu, 2012. Limitations and Potential of Optical and Radar Satellite Imagery to Monitor Environmental Response to Coastal Emergencies in Louisiana, USA. *Journal of Coastal Research*, 28(2):457-476.
- Sasser, C., J. Visser, E. Mouton, J. Linscombe, and S. Hartley, 2008. Vegetation Types in Coastal Louisiana in 2007. U.S. Geological Survey Open-File Report 2008-1224, <http://pubs.usgs.gov/of/2008/1224>, accessed July 2011.
- Schaber, J. and F. Badeck, 2003. Physiology-Based Phenology Models for Forest Tree Species in Germany. *International Journal of Biometeorology* 47:193-201.
- Smith, L., 1997. Satellite Remote Sensing of River Inundation Area, Stage, and Discharge: A Review. *Hydrological Processes* 11:1427-1439.
- SONRIS (Strategic Online Natural Resources Information System), 2009. SONRIS Integrated Applications. Louisiana Department of Natural Resources, Baton Rouge, Louisiana. http://sonris-www.dnr.state.la.us/www_root/sonris_portal_1.htm, accessed August 2011.
- Symbios Spazio, 2010. The Earth Observation Handbook, Climate Change Special Edition. Committee on Earth Observation Satellites (CEOS). <http://www.eohandbook.com>, accessed April 2013.
- Töyra, J. and A. Pietroniro, 2005. Towards Operational Monitoring of a Northern Wetland Using Geomatics-Based Techniques. *Remote Sensing of Environment* 97:174-191.
- Wang, Y., 2004. Seasonal Change in the Extent of Inundation on Floodplains Detected by JERS-1 Synthetic Aperture Radar Data. *International Journal of Remote Sensing* 25(13):2497-2508.
- Werle, D., T. Martin, and K. Hasan, 2000. Flood and Coastal Zone Monitoring in Bangladesh with Radarsat ScanSAR: Technical Experience and Institutional Challenges. *Johns Hopkins APL Technical Digest* 21(1):148-154.